

Generalized L_p -norm joint inversion of gravity and magnetic data using cross-gradient constraint

Saeed Vatankehah ^{1,2}, Shuang Liu ¹, Rosemary A. Renaut ³, Xiangyun Hu ¹,
Mostafa Gharloghi ²

¹ *Hubei Subsurface Multi-scale Imaging Key Laboratory, Institute of Geophysics and Geomatics, China University of Geosciences, Wuhan, China*

² *Institute of Geophysics, University of Tehran, Tehran, Iran*

³ *School of Mathematical and Statistical Sciences, Arizona State University, Tempe, AZ, USA*

SUMMARY

A generalized unifying approach for L_p -norm joint inversion of gravity and magnetic data using the cross-gradient constraint is presented. The presented framework incorporates stabilizers that use L_0 , L_1 , and L_2 -norms of the model parameters, and/or the gradient of the model parameters. Furthermore, the formulation is developed from standard approaches for independent inversion of single data sets, and, thus, also facilitates the inclusion of necessary model and data weighting matrices that provide, for example, depth weighting and imposition of hard constraint data. The developed efficient algorithm can, therefore, be employed to provide physically-relevant smooth, sparse, or blocky target(s) which are relevant to the geophysical community. Here, the nonlinear objective function, that describes the inclusion of all stabilizing terms and the fit to data measurements, is minimized iteratively by imposing stationarity on the linear equation that results from applying linearization

of the objective function about a starting model. To numerically solve the resulting linear system, at each iteration, the conjugate gradient (CG) algorithm is used. The general framework is then validated for three-dimensional synthetic models for both sparse and smooth reconstructions, and the results are compared with those of individual gravity and magnetic inversions. It is demonstrated that the presented joint inversion algorithm is practical and significantly improves reconstructed models obtained by independent inversion.

Key words:

1 INTRODUCTION

Potential field surveys, gravity and magnetic, have been reported as effective strategies for delineating subsurface geological targets. They are applied in a wide range of studies including, for example, oil and gas exploration, mining applications, and mapping the basement topography (Nabighian et al. 2005; Blakely 1996). These surveys are relatively cheap, non-destructive passive remote sensing methods, and can provide valuable information of the subsurface targets. Yet, they only require the measurement of variations in the Earth's natural fields that are caused by changes in the physical properties of the subsurface rocks. In the interpretation process, the acquired survey data can be used in an automatic inversion algorithm for estimation of specific parameters of a subsurface target, for example its geometry or physical properties. It is well known, however, that the potential field inversion problem is ill posed. Identifiability of stable and physically-relevant solutions is then obtained by application of suitable regularization strategies. An independent solution of the inverse problem for either gravity, or magnetic, data for the survey area will only provide information about the density or susceptibility, respectively, of the subsurface. On the other hand, complementary solution of the inverse problem for both data sets can be used to reveal both density and magnetization variations present in a subsurface target. Thus, it is more appropriate to perform a simultaneous joint inversion that uses both data sets. Combined with regularization, this is an effective strategy for yielding a reliable subsurface geological model, that simplifies the interpretation of the subsurface target(s). Thus, the development of efficient and stable joint inversion algorithms has received increased attention in the geophysical community.

Many different techniques have been developed for the simultaneous joint inversion of geophysical data sets. Generally, these techniques can be categorized into two main groups:

(i) petrophysical, and (ii) structural approaches. Petrophysical techniques rely on a direct relationship between two or more physical properties of the subsurface target, for example the assumption that the resistivity and the velocity are both functions of porosity and water saturation (Gallardo & Meju 2003). Although, this strategy is attractive, it does depend on finding a reliable empirical relationship between physical properties. This is a difficult task for general geological media because there is usually no simple or single relationship that approximates the whole range of effects (Gallardo & Meju 2003). Further discussion of the details of the application of petrophysical techniques for joint inversion is provided in the literature, including for example in Nielson & Jacobsen (2000) and Moorkamp et al. (2011; 2013). Structural approaches use, instead, the model topology in order to enhance the structural similarity of reconstructed models (Haber & Oldenburg 1997; Gallardo & Meju 2003; Gallardo & Meju 2004; Tryggvason & Linde 2006; Fregoso & Gallardo 2009). The main idea is that changes, at any point in the different models, should occur in the same or opposite spatial directions, or alternatively, changes will only occur in one of the models. Mathematically, this may be achieved by forcing the cross product of the gradient of the different model parameters to be zero everywhere (Gallardo & Meju 2003; Gallardo & Meju 2004; Tryggvason & Linde 2006). Indeed, many successful results for simultaneous joint inversion with the inclusion of the cross-gradient constraint have been reported, (Gallardo & Meju 2003; Gallardo & Meju 2004; Tryggvason & Linde 2006; Gallardo 2007; Fregoso & Gallardo 2009; Haber & Gazit 2013; Fregoso et al. 2015; Gross 2019; Zhang & Wang 2019). On the other hand, Zhdanov et al. (2012) observed that the Gramian constraint can be used to enhance the correlation between different physical properties and/or their attributes. In this approach, the correlation is enhanced by minimizing the determinant of the Gram matrices of multi-model model parameters during the inversion process. The Gramian constraint approach is general; extant methods based on petrophysical correlations or cross-gradient minimization are special case reductions (Zhdanov et al. 2012). Moreover, unlike the case when performing petrophysical joint inversion, a priori information about the specific relationships between the different physical parameters, or their attributes, is not required. The methodology has been used extensively in the joint inversion of different data sets, see for example Zhdanov (2015), Lin & Zhdanov (2018) and Jorgensen & Zhdanov (2019). In this study we assume that the structure of the subsurface target(s) yields density and susceptibility model parameters over an approximately similar structure. Thus, our focus is on the use of the cross-gradient constraint within a general L_p formulation for efficient simultaneous joint inversion of gravity and magnetic data sets.

Different types of stabilizers have been adopted for the inversion of potential field data, dependent on the desired smoothness, or otherwise, of model features that are to be recovered. For example, it may be appropriate to reconstruct a model which only represents the large-scale features of the subsurface under the survey area without any arbitrary discontinuities. This is achieved with the maximum smoothness stabilizer which uses a L_2 -norm^I of the gradient of the model parameters, (Constable et al. 1987; Li & Oldenburg 1996; Pilkington 1997; Li & Oldenburg 1998). On the contrary, when it is anticipated that the subsurface structure exhibits discontinuities, stabilization can be achieved by imposing the L_1 -norm, or L_0 -norm, on the gradient of the model parameters (Farquharson & Oldenburg 1998; Portniaguine & Zhdanov 1999; Bertete-Aguirre et al. 2002; Vatankehah et al. 2018a; Fournier & Oldenburg 2019). Alternatively, when it can be assumed that the subsurface targets are localized and compact, it is more appropriate to apply the L_1 or L_0 -norms directly on the model parameters (Last & Kubik 1983; Portniaguine & Zhdanov 1999; Barbosa & Silva 1994; Zhdanov & Tolstaya 2004; Ajo-Franklin et al. 2007; Vatankehah et al. 2014a; Vatankehah et al. 2014b; Sun & Li 2014; Zhdanov 2015; Vatankehah et al. 2017). In the potential field literature, stabilization by application of the L_0 -norm on the model parameters is usually referred to as the compactness constraint, whereas application of the L_1 -norm, or L_0 -norm, on the gradient is referred to as total variation (TV) and minimum gradient support (MGS), stabilization, respectively. A unifying approach for application of these constraints for single potential field inversion is presented in Vatankehah et al. (2019a). This approach also includes the modification of the stabilizers to account for additional model and data weighting matrices, such as required for imposition of depth weighting and hard constraint conditions, (Li & Oldenburg 1996; Boulanger & Chouteau 2001). Note that the use of depth weighting counteracts the natural rapid decay of the kernels, dependent on the specific kernel, whether magnetic or gravity. This then facilitates the contribution of all prisms at depth to the surface measurements with an approximately equal probability through the inversion algorithm. The hard constraint weighting is used to impose available geological information on the reconstructed model. Consequently, any practical algorithm for the joint inversion of gravity and magnetic data should also incorporate such weighting schemes. Here, we extend this unifying framework for simultaneous joint inversion of gravity and magnetic data sets in conjunction with the use of the cross-gradient constraint.

The well-known and widely-used formula of Fregoso & Gallardo (2009) for the joint in-

^I The L_p -norm of a vector $\mathbf{x} \in \mathcal{R}^n$ is defined as $\|\mathbf{x}\|_p = (\sum_i^n |x_i|^p)^{1/p}$, $p \geq 1$, and $\|\mathbf{x}\|_0$ counts the number of nonzero entries in \mathbf{x} .

version of gravity and magnetic data, incorporating the cross-gradient constraint, is based on the use computationally of the generalized nonlinear least-squares framework developed by Tarantola & Valette (1982). Here, we wish to include deterministic constraints within the simultaneous joint inversion of the data and thus adopt a deterministic viewpoint for the parameter estimation. The nonlinear objective function, that describes the inclusion of all stabilizing terms and the fit to data measurements, is minimized iteratively by imposing stationarity on the linear equation that results from applying linearization of the objective function about a starting model. To perform the inversion, the iteratively re-weighted least-squares (IRLS) strategy is then used (Wohlberg & Rodriguez 2007). At each iteration, the conjugate gradient (CG) algorithm is applied to numerically solve the resulting linear system.

The paper organized as follow. In Section 2, the theoretical development of the algorithm is presented, along with a unifying framework that makes it possible to combine different types stabilizers within the context of joint inversion. In Section 3, the developed algorithm is validated on synthetic examples. Here, two synthetic models are used; and both sparse and smooth reconstructions are considered. Section 4 is dedicated to a discussion of conclusions and future topics for research.

2 JOINT INVERSION METHODOLOGY

To formulate the problem, we use the well-known strategy for linear inversion of potential field data in which the subsurface is divided into a set of rectangular prisms with fixed size but unknown physical properties (Li & Oldenburg 1996; Boulanger & Chouteau 2001). Here, it is assumed that there is no remanent magnetization, and that self-demagnetization effects are also negligible. For ease of exposition, we first introduce some basic notation for stacking of vectors (matrices) and generation of block diagonal matrices. We use `block_stack(\cdot, \cdot)` to indicate the stacking of vectors (or matrices) with the same number of columns in one vector (or matrix). Further, `block_diag(A, B)` indicates a block diagonal matrix of size $(m_A + m_B) \times (n_A + n_B)$ when A and B are of sizes $(m_A \times n_A)$ and $(m_B \times n_B)$, respectively. Both definitions extend immediately for more than two entities.

We suppose that m measurements are taken for two sets of potential field data ^{II}. These are the vertical components of the gravity and total magnetic fields, and they are stacked in vectors $\mathbf{d}_1^{\text{obs}}$, and $\mathbf{d}_2^{\text{obs}}$, each of length m , respectively. The unknown physical parameters, the

^{II} We could assume different numbers of measurements for each field, m_1 and m_2 but for simplicity of the discussion we immediately assume $m_1 = m_2 = m$.

density and the susceptibility, of n prisms are also stacked in vectors \mathbf{m}_1 , and \mathbf{m}_2 , respectively. The data vectors and model parameters are then stacked consistently in vectors $\mathbf{d}^{\text{obs}} = \text{block_stack}(\mathbf{d}_1^{\text{obs}}, \mathbf{d}_2^{\text{obs}}) \in \mathcal{R}^{2m}$, and $\mathbf{m} = \text{block_stack}(\mathbf{m}_1, \mathbf{m}_2) \in \mathcal{R}^{2n}$. The measurements are connected to the model parameters via $G\mathbf{m} = \mathbf{d}^{\text{obs}}$ where $G = \text{block_diag}(G_1, G_2) \in \mathcal{R}^{2m \times 2n}$, and G_1 and G_2 are the linear forward modeling operators for gravity and magnetic kernels, respectively. There are different alternative formulas which can be used to compute the entries of matrices G_1 and G_2 . Here, we use the formulas developed by Haáz (1953), for computing the vertical gravitational component, and Rao & Babu (1991), for the total magnetic field anomaly, of a right rectangular prism, respectively.

The goal of the inversion is to find geologically plausible models \mathbf{m}_1 and \mathbf{m}_2 that predict $\mathbf{d}_1^{\text{obs}}$ and $\mathbf{d}_2^{\text{obs}}$, respectively, via a simultaneous joint algorithm that also facilitates the incorporation of relevant weighting matrices in the algorithm. We formulate the joint inversion for the determination of the model parameters \mathbf{m}_1 and \mathbf{m}_2 as the minimization of the global objective function, in which parameters α and λ are relative weighting parameters for the respective terms,

$$P^{(\alpha, \lambda)}(\mathbf{m}) = \|W_{\mathbf{d}}(\mathbf{d}^{\text{obs}} - G\mathbf{m})\|_2^2 + \alpha^2 \|WD(\mathbf{m} - \mathbf{m}^{\text{apr}})\|_2^2 + \lambda^2 \|\mathbf{t}(\mathbf{m})\|_2^2. \quad (1)$$

The data misfit term, $\|W_{\mathbf{d}}(\mathbf{d}^{\text{obs}} - G\mathbf{m})\|_2^2$, measures how well the calculated data reproduce the observed data. Diagonal matrix $W_{\mathbf{d}} = \text{block_diag}(W_{\mathbf{d}_1}, W_{\mathbf{d}_2}) \in \mathcal{R}^{2m \times 2m}$, where $W_{\mathbf{d}_1}$ and $W_{\mathbf{d}_2}$ are diagonal weighting matrices for the gravity and magnetic data, respectively. Here we suppose that these diagonal elements are the inverses of the standard deviations of the independent, but potentially colored, noise in the data. Zhang & Wang (2019) considered an alternative weighting based on the individual row norms which could also be used here. The stabilizer, $\|WD(\mathbf{m} - \mathbf{m}^{\text{apr}})\|_2^2$, controls the growth of the solution with respect to the weighted norm, and is especially significant as it determines the structural qualities of the desired solution. Here, this stabilizer is presented through a general L_2 -norm formulation, but we will discuss how different choices of W and D lead to different L_p -norm stabilizations. In (1) the vector $\mathbf{m}^{\text{apr}} = \text{block_stack}(\mathbf{m}_1^{\text{apr}}, \mathbf{m}_2^{\text{apr}}) \in \mathcal{R}^{2n}$ is an initial starting model that maybe known from previous investigations. It is also possible to set $\mathbf{m}^{\text{apr}} = \mathbf{0}$. The link between the gravity and magnetic models in this inversion algorithm is the cross-gradient function $\mathbf{t}(\mathbf{m}) \in \mathcal{R}^{3n}$. For this study, we assume that the model structures for \mathbf{m}_1 and \mathbf{m}_2 are approximately the same, and thus that it is important to measure the structural similarity using the cross-gradient constraint which will be approximately zero for models with similar

structures. We therefore use

$$\mathbf{t}(\mathbf{m}) = \nabla \mathbf{m}_1(x, y, z) \times \nabla \mathbf{m}_2(x, y, z), \quad (2)$$

where ∇ indicates the gradient operator (Gallardo & Meju 2003) and structural similarity is achieved when $\mathbf{t}(\mathbf{m}) = \mathbf{0}$, see Appendix A for details. As noted already in Section 1, this corresponds to the case in which the gradient vectors are in the same or opposite direction, or, alternatively, one of them is zero (Gallardo & Meju 2003; Gallardo & Meju 2004; Tryggvason & Linde 2006; Gallardo 2007; Fregoso & Gallardo 2009; Haber & Gazit 2013; Fregoso et al. 2015). From a geological viewpoint this means that if a boundary exists then it must be sensed by both methods in a common orientation regardless of how the amplitude of the physical property changes (Gallardo & Meju 2003). This means that information that is contained in one model is relevant to the other model and vice versa. Therefore, structures determined by one model can assist with the identification of structures in the other model, and, as a consequence, the structures of the two models can correct each other throughout the joint inversion process (Gallardo & Meju 2003; Haber & Gazit 2013). On the other hand, while it is assumed that both models have similar structures at similar locations, it is also possible for one model to have a structure in a location where the other model has none (Haber & Gazit 2013). Further details about characteristic properties of the cross-gradient constraint are provided in Gallardo & Meju (2003), Tryggvason & Linde (2006), and Fregoso & Gallardo (2009).

The stabilizing term, $\|WD(\mathbf{m} - \mathbf{m}^{\text{apr}})\|_2^2$, in (1) has a very significant impact on the solution that is obtained by minimizing (1). Depending on the type of desired model to be recovered, there are many choices that can be considered for this stabilization, and that have been extensively adopted by the geophysical community. Here, we show how it is possible to use the given weighted L_2 -norm regularizer to approximate different L_p -norm stabilizers, $0 \leq p \leq 2$, (Vatankhah et al. 2019a). Suppose D is the identity matrix, $D = I_{2n}$, and W is selected as $W = \text{block_diag}(W_1, W_2) \in \mathcal{R}^{2n \times 2n}$, in which,

$$W_i = (W_{\text{depth}})_i (W_{\text{h}})_i (W_{L_p})_i \in \mathcal{R}^{n \times n}, \quad i = 1, 2. \quad (3)$$

Here, the diagonal weighting matrix $(W_{L_p})_i \in \mathcal{R}^{n \times n}$ is defined, assuming entries are calculated elementwise, by

$$(W_{L_p})_i = \text{diag} \left(1 / ((\mathbf{m}_i - \mathbf{m}_i^{\text{apr}})^2 + \epsilon^2)^{(2-p)/4} \right), \quad i = 1, 2. \quad (4)$$

When $p = 0$ and $p = 1$, compact L_0 -norm and L_1 -norm solutions are obtained, respectively. The choice $p = 2$ provides the L_2 -norm solution of the model parameters. The parameter ϵ is

a small positive number, $0 < \epsilon \ll 1$, which is added to avoid the possibility of division by zero, and has an important effect on the solution. When ϵ is very small the solutions are sparse, while for large values the solutions are smooth. Further discussion on the impact of ϵ is given, for example, in Last & Kubik (1983), Farquharson & Oldenburg (1998), Zhdanov & Tolstaya (2004), Ajo-Franklin et al. (2007), Fiandaca et al. (2015), and Fournier & Oldenburg (2019). On the other hand, it is also possible to chose D to provide an approximation to the gradient of the model parameters. Suppose, for example, that $D_1 = \text{block_stack}(D_x, D_y, D_z) \in \mathcal{R}^{3n \times n}$, where D_x , D_y , and D_z are square and provide discrete approximations for derivative operators in x , y , and z -directions. Then, defining $\mathbf{0}_{3n \times n}$ to be the zero matrix of size $3n \times n$, and setting $D_2 = D_1$, we can use the matrix

$$D = \begin{pmatrix} D_1 & \mathbf{0}_{3n \times n} \\ \mathbf{0}_{3n \times n} & D_2 \end{pmatrix} \in \mathcal{R}^{6n \times 2n}, \quad (5)$$

so that $D\mathbf{m}$ yields the approximate gradient of \mathbf{m} . More details about the structure of the matrices D_x , D_y , and D_z can be found in Li & Oldenburg (2000), Lelièvre & Oldenburg (2009), and Lelièvre & Oldenburg (2013). Then, with this definition for D , and again using element-wise calculations, $(W_{L_p})_i$ in (4) is replaced by

$$(W_{L_p})_i = \text{diag} \left(1 / \left((D_x(\mathbf{m} - \mathbf{m}_i^{\text{apr}}))^2 + (D_y(\mathbf{m} - \mathbf{m}_i^{\text{apr}}))^2 + (D_z(\mathbf{m} - \mathbf{m}_i^{\text{apr}}))^2 + \epsilon^2 \right)^{(2-p)/4} \right). \quad (6)$$

But now, for the multiplication in equation (1) to be dimensionally consistent, W is replaced by

$$W = \text{block_diag}(W_1, W_1, W_1, W_2, W_2, W_2) \in \mathcal{R}^{6n \times 6n}. \quad (7)$$

In the definition of $(W_{L_p})_i$, given in (6), picking $p = 2$ produces a solution with minimum structure yielding a smooth model without arbitrary discontinuities (Constable et al. 1987; Li & Oldenburg 1996; Pilkington 1997). If we anticipate that there are true discontinuous jumps, then, it is possible to take $p = 1$ or $p = 0$ for a total variation (TV) or minimum gradient support (MGS) stabilization, respectively. In summary, all aforementioned definitions indicate how, dependent on the choices of p and D in W , it is possible to use the objective function (1) with a desired stabilizer. Well-known stabilizers, including TV, MGS, minimum structure, compactness, and L_1 -norm can all be incorporated in a joint inversion methodology. Moreover, this unifying framework allows the use of additional stabilizers, which are not common in potential field inversion, simply by changing the choice of p .

In (3), the diagonal depth weighting matrix, $(W_{\text{depth}})_i = \text{diag}(1/(z_j + z_0)^{\beta_i})$ is used to

counteract the rapid decay of the kernel with depth (Li & Oldenburg 1996; Pilkington 1997). Here z_j is the mean depth of prism j , z_0 depends both upon prism size and the height of the observed data. With application of appropriate depth weighting, as determined by parameter β_i , all prisms participate with an approximately equal probability in the inversion process. The diagonal hard constraint matrix $(W_h)_i$, is generally an identity matrix. If geological information, or prior investigations in the survey area, can provide the values of the model parameter for some prisms, then, the information is included in $\mathbf{m}_i^{\text{apr}}$, and the corresponding diagonal entries of $(W_h)_i$ are set to a large value (Boulangier & Chouteau 2001; Vatankhah et al. 2014a; Vatankhah et al. 2018b). These known parameters are kept fixed during the iterative minimization of (1). Equivalently, the inversion algorithm searches only for unknown model parameters. As an important aside, note that all matrices D_x , D_y , D_z , W_{depth} , W_h , and W_{L_p} , are sparse and can therefore be saved using a MATLAB `sparse` format, with very limited demand on the memory.

Now, in (1) both W_{L_p} and $\mathbf{t}(\mathbf{m})$ depend on the model parameters \mathbf{m} . Thus, the objective function (1) is nonlinear with respect to \mathbf{m} . We use a simple iterative strategy to convert $P^{(\alpha,\lambda)}(\mathbf{m})$ to a linear form, in which to linearize the cross-gradient constraint, the first order Taylor expansion is used (Gallardo & Meju 2003; Gallardo & Meju 2004; Tryggvason & Linde 2006; Gallardo 2007; Fregoso & Gallardo 2009). First, suppose that the superscript ℓ applied to any variable indicates the value of that variable at iteration ℓ , so that $\mathbf{m}^{(\ell)}$ is the estimate of the model parameters at iteration ℓ . Then, we suppose that $\mathbf{m}^{(1)} = \mathbf{m}^{\text{apr}}$ and rewrite the objective function (1) as

$$P^{(\alpha,\lambda)}(\mathbf{m}) = \|W_d(\mathbf{d}^{\text{obs}} - G\mathbf{m})\|_2^2 + \alpha^2 \|W^{(\ell-1)}D(\mathbf{m} - \mathbf{m}^{(\ell-1)})\|_2^2 \quad (8)$$

$$+ \lambda^2 \|\mathbf{t}^{(\ell-1)} + \mathbf{B}^{(\ell-1)}(\mathbf{m} - \mathbf{m}^{(\ell-1)})\|_2^2, \quad \ell = 2, 3, \dots$$

Note that $W^{(\ell-1)}$ indicates W estimated at iteration $\ell - 1$ through the nonlinear definition for W_{L_p} as given in (4) or (6). Here, $\mathbf{t}^{(\ell-1)}$ and $\mathbf{B}^{(\ell-1)} = (\nabla_{\mathbf{m}}\mathbf{t}^{(\ell-1)})$ are the cross-gradient and the Jacobian matrix of the discrete approximation for the cross-gradient function, respectively, evaluated at $\mathbf{m}^{(\ell-1)}$, consistent with the linear Taylor expansion for \mathbf{t} around $\mathbf{m}^{(\ell-1)}$. The formulae used are given in Appendix A. Taking $\nabla_{\mathbf{m}}P^{(\alpha,\lambda)}(\mathbf{m}) = \mathbf{0}$ defines the update $\mathbf{m}^{(\ell)}$ as the solution of

$$-G^T W_d^T W_d(\mathbf{d}^{\text{obs}} - G\mathbf{m}) + \alpha^2 D^T (W^{(\ell-1)})^T W^{(\ell-1)} D(\mathbf{m} - \mathbf{m}^{(\ell-1)}) + \quad (9)$$

$$\lambda^2 \left((\mathbf{B}^{(\ell-1)})^T \left\{ \mathbf{t}^{(\ell-1)} + \mathbf{B}^{(\ell-1)}(\mathbf{m} - \mathbf{m}^{(\ell-1)}) \right\} \right) = 0.$$

Then, after some algebraic manipulation, the desired update for \mathbf{m} is given by

$$\mathbf{m}^{(\ell)} = \mathbf{m}^{(\ell-1)} + \Delta\mathbf{m}^{(\ell-1)}, \quad (10)$$

where $\Delta\mathbf{m}^{(\ell-1)}$ is the solution of the equation

$$\begin{aligned} & \left(G^T W_{\mathbf{d}}^T W_{\mathbf{d}} G + \alpha^2 D^T (W^{(\ell-1)})^T W^{(\ell-1)} D + \lambda^2 (\mathbf{B}^{(\ell-1)})^T \mathbf{B}^{(\ell-1)} \right) \Delta\mathbf{m}^{(\ell-1)} = \\ & \left(G^T W_{\mathbf{d}}^T W_{\mathbf{d}} (\mathbf{d}^{\text{obs}} - G\mathbf{m}^{(\ell-1)}) - \lambda^2 (\mathbf{B}^{(\ell-1)})^T \mathbf{t}^{(\ell-1)} \right). \end{aligned} \quad (11)$$

Equivalently, defining

$$E^{(\ell)} = \left(G^T W_{\mathbf{d}}^T W_{\mathbf{d}} G + \alpha^2 D^T (W^{(\ell-1)})^T W^{(\ell-1)} D + \lambda^2 (\mathbf{B}^{(\ell-1)})^T \mathbf{B}^{(\ell-1)} \right), \quad (12)$$

and

$$\mathbf{f}^{(\ell)} = \left(G^T W_{\mathbf{d}}^T W_{\mathbf{d}} (\mathbf{d}^{\text{obs}} - G\mathbf{m}^{(\ell-1)}) - \lambda^2 (\mathbf{B}^{(\ell-1)})^T \mathbf{t}^{(\ell-1)} \right), \quad (13)$$

then $\Delta\mathbf{m}^{(\ell-1)}$ given by (11) solves the linear system $E^{(\ell)}\Delta\mathbf{m}^{(\ell-1)} = \mathbf{f}^{(\ell)}$. Numerically the CG algorithm can be used to solve (11) and a line search can also be included in the update (10), replacing $\Delta\mathbf{m}^{(\ell-1)}$ by $\gamma^{(\ell-1)}\Delta\mathbf{m}^{(\ell-1)}$ where $0 < \gamma^{(\ell-1)}$ is chosen to speed convergence, see for example Fournier & Oldenburg (2019). We should note that at each iteration of the algorithm lower and upper bounds on density and susceptibility are imposed. During the inversion process if an estimated physical property falls outside the specified bounds, it will be returned back to the nearest bound. Further, to test the convergence of the solution at each iteration ℓ , we calculate a χ^2 measure for the respective data fit term at each iteration,

$$(\chi_i^2)^{(\ell)} = \|W_{\mathbf{d}_i}(\mathbf{d}_i^{\text{obs}} - G_i\mathbf{m}_i^{(\ell)})\|_2^2, \quad i = 1, 2. \quad (14)$$

The iteration will terminate at convergence only when $(\chi_i^2)^{(\ell)} \leq m + \sqrt{2m}$, for both $i = 1$, and $i = 2$. Otherwise, the iteration is allowed to proceed to a maximum number of iterations MAXIT. The steps of the joint inversion algorithm are summarized in Algorithm 1.

In (1) the important parameters α and λ are the regularization parameters which give relative weights to the stabilizer and the cross-gradient term, respectively. To be more precise, we define α as $\text{block_diag}(\alpha_1 I_n, \alpha_2 I_n) \in \mathcal{R}^{2n \times 2n}$, where α_1 and α_2 are the relative weights for the gravity and magnetic terms, respectively. We should note that, although α is a diagonal matrix and can be used inside the stabilizer, we prefer to put α outside in order for the formulation to be consistent with the conventional Tikhonov objective functional. Weighting parameters α_1 , α_2 , and λ have an important effect on the estimated solution. Thus, they need to be determined carefully. But application of an automatic parameter-choice method for determining α_1 , α_2 , and λ is difficult, or potentially impossible, and is outside the scope of this

current study. Therefore we adopt a simple but practical strategy for determining suitable values of these parameters. Previous investigations have demonstrated that it is efficient if the inversion starts with a large regularization parameter (Farquharson & Oldenburg 2004; Vatanikhah et al. 2014a). We follow that strategy here and start the inversion with large α_1 and α_2 . In subsequent iterations the parameters are reduced slowly dependent on parameters q_1 and q_2 , respectively, using $\alpha_1^{(\ell)} = \alpha_1^{(\ell-1)} q_1$ and $\alpha_2^{(\ell)} = \alpha_2^{(\ell-1)} q_2$, where q_1 and q_2 are small numbers, $0 \ll q_1, q_2 < 1$. The process continues until the predicted data of one of the reconstructed models satisfies the observed data at the noise level. For that data set, the relevant parameter is then kept fixed during the following iterations. The parameter λ is held fixed in the implementation, although it is quite feasible that it is also iteration dependent. The amount of structural similarity obtained through the joint inversion algorithm can be adjusted using different choices of λ . The impact of selecting the parameters α_1 , α_2 , (equivalently q_1 and q_2), and λ is demonstrated in Section 3.

3 SIMULATIONS

The validity of the presented joint inversion algorithm is evaluated for synthetic examples and the results are compared with those of the separate gravity and magnetic inversions. We select a model that consists of two dikes, one is a small vertical dike and the other is a larger dipping dike. In the first study, we suppose that the targets have both a density contrast and a susceptibility distribution. The density contrast and the susceptibility of the targets are selected as $\rho = 0.6 \text{ gr cm}^{-3}$ and $\kappa = 0.06$ (SI unit), respectively, embedded in a homogeneous non-susceptible background. For the second study, we assume that the dipping dike has a density and susceptibility distribution, but that the vertical dike is not magnetic. For all inversions, the bound constraints $0 = \rho_{\min} \leq \mathbf{m}_1 \leq \rho_{\max} = 0.6, \text{ gr cm}^{-3}$, and $0 = \kappa_{\min} \leq \mathbf{m}_2 \leq \kappa_{\max} = 0.06, \text{ SI unit}$, are imposed. To generate the total field anomaly, the intensity of the geomagnetic field, the inclination, and the declination are selected as 50000 nT, 45° and 45° , respectively. To simulate realistic noise-contaminated observed data, we suppose that Gaussian noise with zero mean and standard deviations $(\tau_1 |(\mathbf{d}_i^{\text{exact}})_j| + \tau_2 \max(|\mathbf{d}_i^{\text{exact}}|))$, $j = 1 \dots n$, are added to each exact true measurement j , $(\mathbf{d}_i^{\text{exact}})_j$. The parameters pairs (τ_1, τ_2) are selected as (0.02, 0.012) and (0.02, 0.01) for gravity and magnetic data, respectively. These standard deviations are selected such that the signal to noise ratios (SNR), as given by

$$\text{SNR}_i = 20 \log_{10} \left(\frac{\|\mathbf{d}_i^{\text{exact}}\|_2}{\|\mathbf{d}_i^{\text{obs}} - \mathbf{d}_i^{\text{exact}}\|_2} \right), \quad i = 1, 2, \quad (15)$$

Algorithm 1 Generalized L_p -norm joint inversion of gravity and magnetic data.

Input: \mathbf{d}^{obs} , \mathbf{m}^{apr} , G , $W_{\mathbf{d}}$, $(W_{\mathbf{h}})_1$, $(W_{\mathbf{h}})_2$, D_x , D_y , D_z , ϵ , ρ_{\min} , ρ_{\max} , κ_{\min} , κ_{\max} , MAXIT, β_1 , β_2 , $\alpha_1^{(1)}$, $\alpha_2^{(1)}$, q_1 , q_2 and λ .

- 1: Calculate $(W_{\text{depth}})_1$ and $(W_{\text{depth}})_2$ as determined by β_1 and β_2 , respectively.
- 2: Set $W_1 = (W_{\text{depth}})_1(W_{\mathbf{h}})_1$ and $W_2 = (W_{\text{depth}})_2(W_{\mathbf{h}})_2$.
- 3: If D is the identity form $W = \text{block_diag}(W_1, W_2)$. Otherwise set $W = \text{block_diag}(W_1, W_1, W_1, W_2, W_2, W_2)$.
- 4: Initialize $\mathbf{m}^{(1)} = \mathbf{m}^{\text{apr}}$, $(W_{L_p})_1^{(1)} = I$, $(W_{L_p})_2^{(1)} = I$, and $\ell = 1$.
- 5: **while** Not converged, noise level not satisfied, and $\ell < \text{MAXIT}$ **do**
- 6: $\ell = \ell + 1$.
- 7: Compute $\mathbf{t}^{(\ell-1)}$ and $\mathbf{B}^{(\ell-1)}$, as given in Appendix A.
- 8: Use CG to solve $E^{(\ell)}\Delta\mathbf{m}^{(\ell-1)} = \mathbf{f}^{(\ell)}$ for $\mathbf{m}^{(\ell-1)}$, defined by (12) and (13).
- 9: Update $\mathbf{m}^{(\ell)} = \mathbf{m}^{(\ell-1)} + \Delta\mathbf{m}^{(\ell-1)}$.
- 10: Impose constraints on $\mathbf{m}^{(\ell)}$ to force $\rho_{\min} \leq \mathbf{m}_1^{(\ell)} \leq \rho_{\max}$ and $\kappa_{\min} \leq \mathbf{m}_2^{(\ell)} \leq \kappa_{\max}$.
- 11: Test convergence criteria, (14), for χ_1^2 and χ_2^2 . Exit loop if both satisfied.
- 12: Set $\alpha_1^{(\ell)} = \alpha_1^{(\ell-1)}q_1$ and $\alpha_2^{(\ell)} = \alpha_2^{(\ell-1)}q_2$. Update $\alpha^{(\ell)}$.
- 13: Determine $(W_{L_p})_1^{(\ell)}$ and $(W_{L_p})_2^{(\ell)}$, dependent on D and p , equations (4) or (6).
- 14: Set $W^{(\ell)} = \text{block_diag}(W_1^{(\ell)}, W_2^{(\ell)})$ when D is the identity. Otherwise set $W^{(\ell)} = \text{block_diag}(W_1^{(\ell)}, W_1^{(\ell)}, W_1^{(\ell)}, W_2^{(\ell)}, W_2^{(\ell)}, W_2^{(\ell)})$
- 15: **end while**

Output: Solution $\rho = \mathbf{m}_1^{(\ell)}$, $\kappa = \mathbf{m}_2^{(\ell)}$, IT = ℓ .

become nearly the same. The resulting SNRs are indicated in the captions of the respective figures associated with the results for the given data set. In all simulations we use $\beta_1 = 0.8$ and $\beta_2 = 1.4$ in $(W_{\text{depth}})_1$ and $(W_{\text{depth}})_2$, respectively. The maximum number of iterations of the algorithm is selected as MAXIT = 100 for all inversions. Further, in the following, we present the results for two different stabilizers; the L_1 -norm of the model parameters imposed using $D = I$ and $p = 1$ in (4), and the minimum structure stabilizer, imposed using $p = 2$ and $D \neq I$ in (6). This then demonstrates the validity of the algorithm for both sparse and smooth reconstructions of the subsurface targets. Focusing parameter ϵ is held fixed in all inversions, $\epsilon^2 = 1e^{-9}$. A summary of the parameters chosen for the simulations discussed in Sections 3.1-3.2 are provided in Table 1.

| Model | Case | Figure | p | D | $\alpha_1^{(1)}$ | q_1 | $\alpha_2^{(1)}$ | q_2 | λ | MAXIT | W_h | Results |
|-------|------|--------|-----|-----|------------------|-------|------------------|-------|-----------|-------|-------|---------|
| 1 | 1 | 1 | 1 | I | 20,000 | 0.9 | 50,000 | 0.95 | 0 | 100 | - | 3 |
| 1 | 2 | 1 | 1 | I | 20,000 | 0.9 | 50,000 | 0.95 | 10^6 | 100 | - | 6 |
| 1 | 2 | 1 | 1 | I | 20,000 | 0.9 | 50,000 | 0.95 | 10^{12} | 100 | - | 9 |
| 1 | 3 | 1 | 1 | I | 20,000 | 0.9 | 50,000 | 0.95 | 10^6 | 100 | Yes | 12 |
| 1 | 4 | 1 | 2 | D | 200,000 | 0.9 | 500,000 | 0.95 | 10^7 | 100 | - | 13 |
| 2 | 1 | 16 | 1 | I | 20,000 | 0.9 | 50,000 | 0.95 | 10^6 | 100 | - | 18 |
| 2 | 2 | 16 | 2 | D | 200,000 | 0.9 | 500,000 | 0.95 | 10^7 | 100 | - | 19 |

Table 1. Summary of the parameters chosen for each of the synthetic simulations that are discussed in Sections 3.1 and 3.2. The true cross section of the models are provided in the figure indicated by the number in the column with heading Figure. The obtained cross sections by the inversion are illustrated in the figure with number in the column with heading Results.

3.1 Model study 1

The first model is illustrated in Fig. 1. The top depths of the bodies are located at 50 m. The dipping dike is extended to 300 m, but the maximum depth of the small vertical dike is 200 m. The data on the surface are generated on a grid with $25 \times 20 = 500$ points and grid spacing 50 m. The noise-contaminated gravity and magnetic data are illustrated in Figs. 2(a) and 2(b), respectively. To perform the inversion, the subsurface volume is discretized into 4000 prisms of sizes 50 m in each dimension. The initial regularization parameters are selected as $\alpha_1^{(1)} = 20,000$ and $\alpha_2^{(1)} = 50,000$. In Vatankeh et al. (2019b) we demonstrated that the gravity and magnetic sensitivity matrices, G_1 and G_2 , have different spectral properties and, therefore, the regularization parameter should be much larger for the inversion of magnetic data as compared to that used for the inversion of gravity data. Thus, it is appropriate to control the speed of convergence for each model with parameters $q_1 = 0.9$ and $q_2 = 0.95$, that are different.

3.1.1 Case 1: separate L_1 -norm inversion

We first implement the algorithm using the L_1 -norm stabilizer but without using the cross-gradient constraint. This is easy to do by selecting $\lambda = 0$. Hence the algorithm proceeds exactly as in Algorithm 1, with the same termination criteria, but without the cross-gradient term. The inversion is initiated using $\mathbf{m}^{\text{apr}} = \mathbf{0}$. After $IT = 61$ iterations the convergence criteria, χ_1^2 and χ_2^2 , are satisfied and the inversion terminates. In this simulation the χ_2^2 termination is

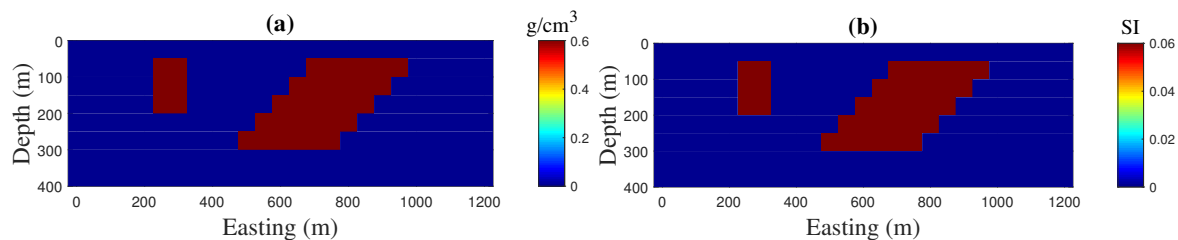


Figure 1. Cross-section of the synthetic model that consists of a vertical and a dipping dike. (a) Density distribution; (b) Susceptibility distribution.

reached at iteration 43. The susceptibility model is recovered more quickly than the density model, which requires additional iterations until both termination criteria are satisfied.

The reconstructed density and susceptibility models are illustrated in Figs. 3(a) and 3(b), respectively. They are in good agreement with the original models, and are acceptable. The results are very close to those that can be obtained using another single L_1 -norm algorithm, see Vatankhah et al. (2019b), in which the unbiased predictive risk estimator is used as parameter-choice method and the singular value decomposition (SVD) is used computationally. It is clear that sharp and focused images of the subsurface are obtained, but the recovered susceptibility model shows more extension in depth for both targets. Further, in the density model, the extension of the vertical dike is underestimated. For comparison, we present the data produced by the models in Figs. 4(a) and 4(b), respectively. In addition, the the progression of the data misfit, the regularization term, and the regularization parameter, with iteration ℓ , for both gravity and magnetic problems, are illustrated in Fig. 5.

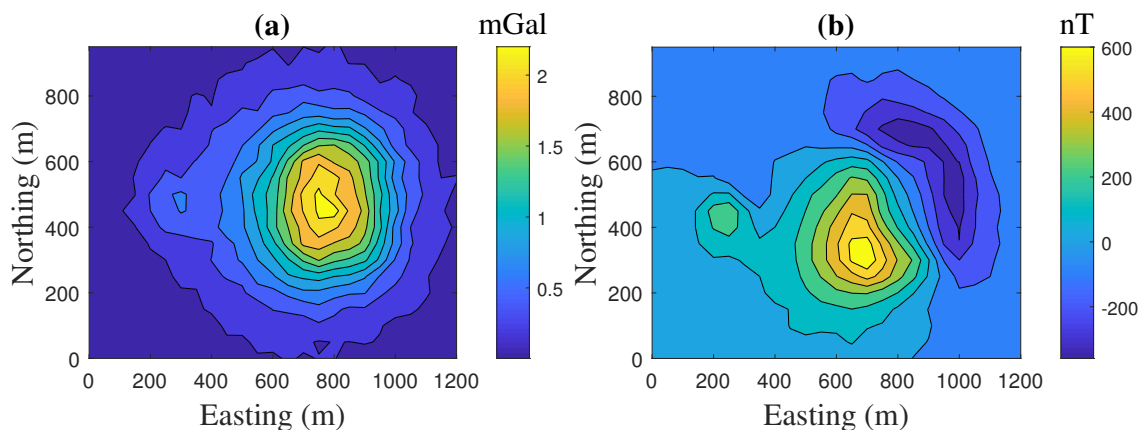


Figure 2. Noise contaminated anomaly produced by the model shown in Fig. 1. (a) Vertical component of gravity; (b) Total magnetic field. The SNR for gravity and magnetic data, respectively, are 25.1778 and 25.1558.

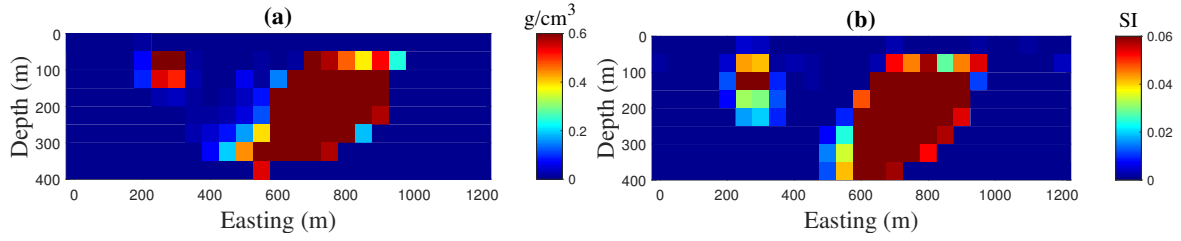


Figure 3. Cross-section of the reconstructed model using individual inversions, Case 1. (a) Density distribution; (b) Susceptibility distribution.

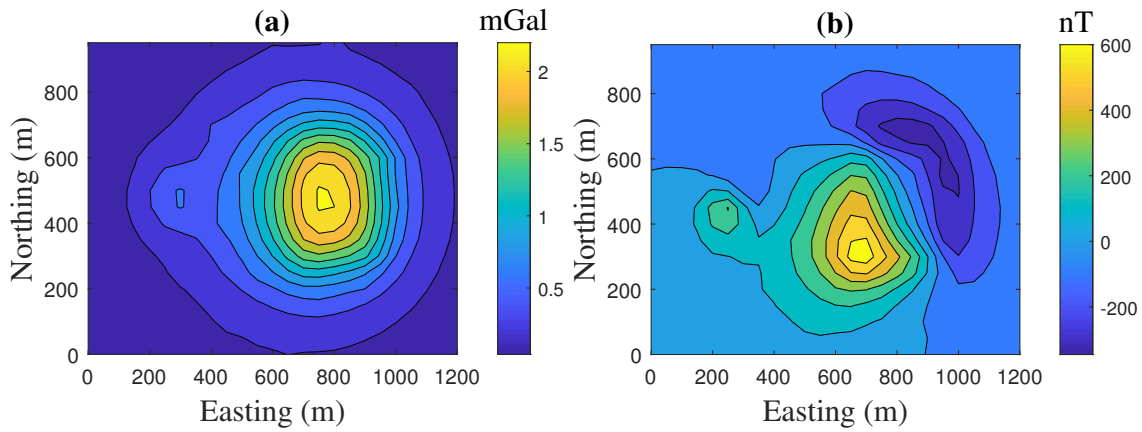


Figure 4. The data produced by the models shown in Fig. 3, Case 1. (a) Vertical component of gravity; (b) Total magnetic field.

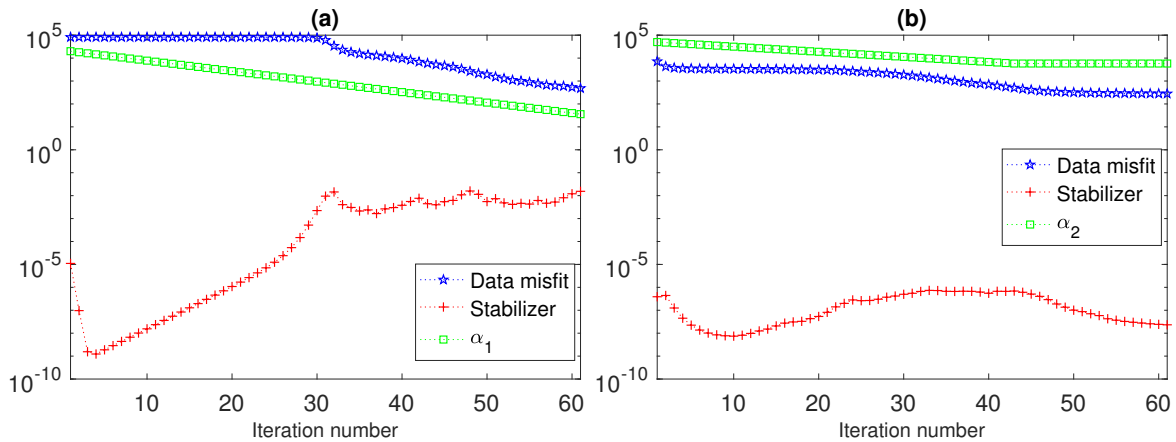


Figure 5. The progression of the data misfit, the regularization term, and the regularization parameter, with iteration ℓ , for the models shown in Fig. 3, Model 1 and Case 1. (a) Gravity inversion; (b) Magnetic inversion.

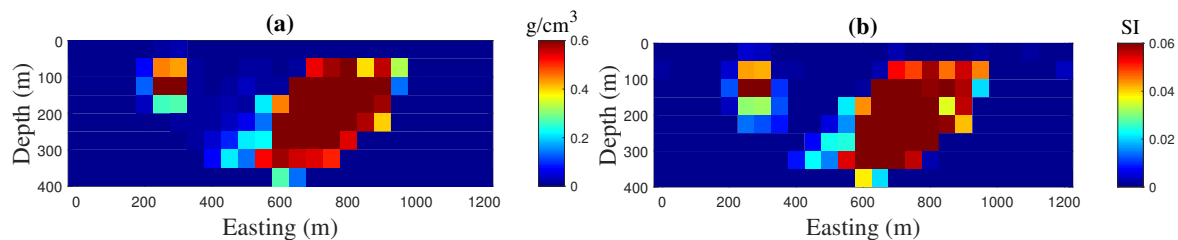


Figure 6. Reconstructed models using joint inversion with $\lambda = 10^6$ and with the L_1 -norm of the model parameters as the stabilizer, Model 1 and Case 2. (a) Density distribution; (b) Susceptibility distribution.

3.1.2 Case 2: joint L_1 -norm inversion with cross-gradient constraint

We now implement the inversion algorithm using the cross-gradient constraint with $\lambda = 10^6$. This selection is based on an analysis of entries of matrix \mathbf{B} , which are very small. If we want to give enough weight to the cross-gradient term, it is necessary to use a large value for λ . We will also show, on the other hand, that if λ is too large the results can be unsatisfactory. All other parameters are selected as for the simulation for Model 1 and Case 1, in Section 3.1.1. The inversion terminates at iteration $IT = 59$, two iterations less than required for the presented individual inversions. The results are presented in Figs. 6, 7, and 8, respectively. Now, the reconstructed density and susceptibility models are quite similar, and are close to the original models. Indeed, the results indicate that the application of the cross-gradient function significantly improves the quality of the solutions. Both targets are in better agreement with the original models.

We next perform the same simulation but select the weighting on the cross-gradient to be

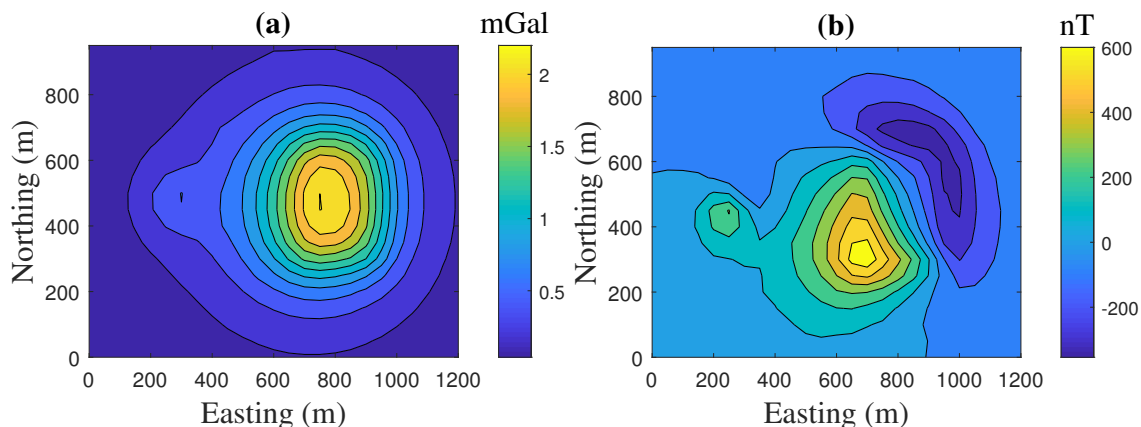


Figure 7. The data produced by the models shown in Fig. 6, Model 1 and Case 2. (a) Vertical component of gravity; (b) Total magnetic field.

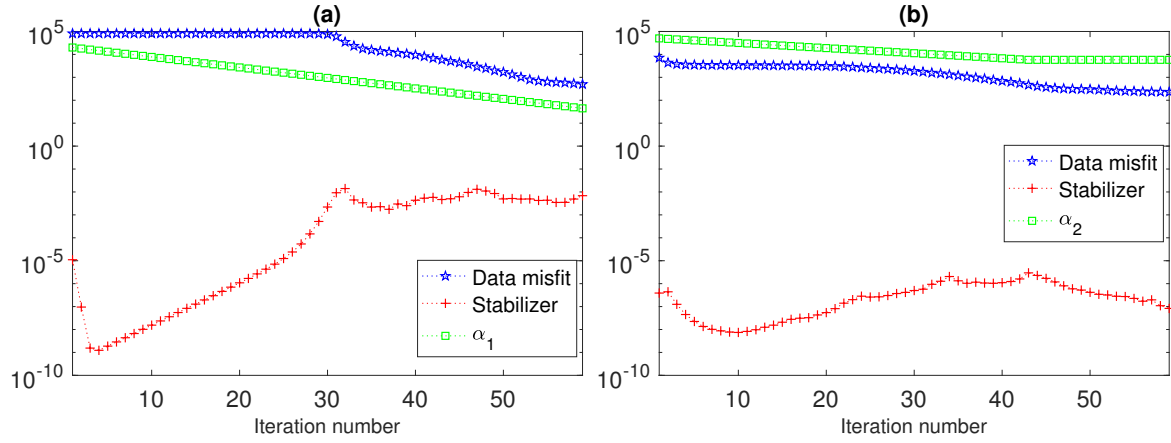


Figure 8. The progression of the data misfit, the regularization term, and the regularization parameter, with iteration ℓ , for the models shown in Fig. 6, Model 1 and Case 2. (a) Gravity; and (b) Magnetic.

very large, with $\lambda = 10^{12}$. In this case, the inversion terminates at $\text{MAXIT} = 100$, without satisfying the noise levels. That means that it is not possible to satisfy the data misfit criteria with a large λ . The results are presented in Figs. 9, 10, and 11. The reconstructed models are not at all consistent with the original models, either with respect to the shape or to the maximum values of the physical properties, especially for reconstruction of the density. Although, the main reconstructed bodies are quite similar to each other, as expected due to the strong requirement imposed by the use of the cross-gradient constraint, some additional unrealistic structures appear in the density model. Clearly the selection of λ is very important. But, this is not a difficult task. It is sufficient to consider the entries of \mathbf{B} , or to run the algorithm once, to determine a suitable λ .

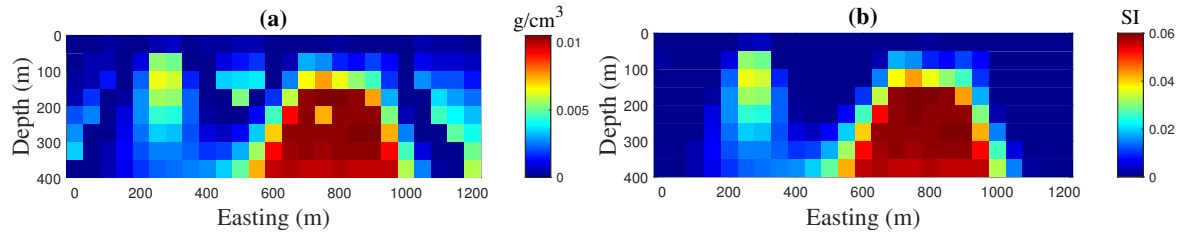


Figure 9. Reconstructed models using joint inversion with $\lambda = 10^{12}$ and with the L_1 -norm of the model parameters as the stabilizer, Model 1 and Case 2. (a) Density distribution; (b) Susceptibility distribution.

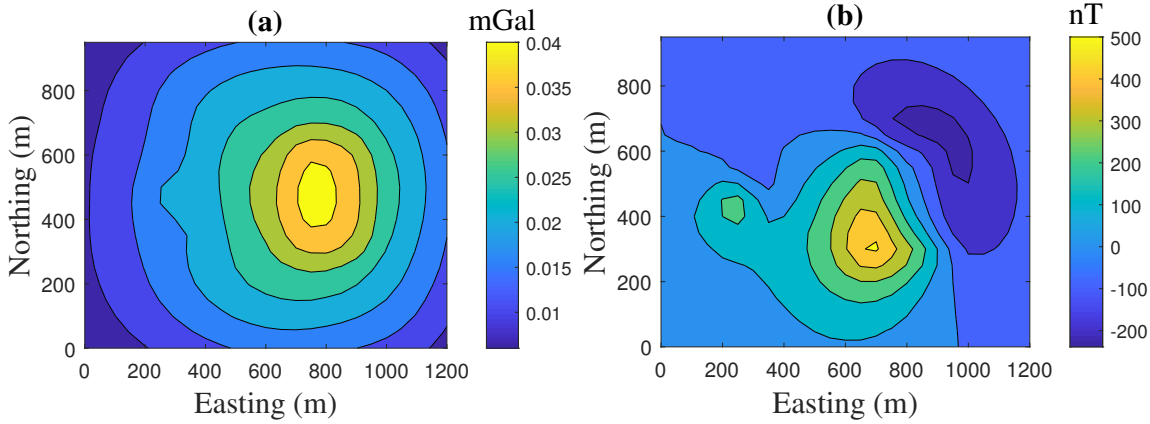


Figure 10. The data produced by the models shown in Fig. 9, Model 1 and Case 2. (a) Vertical component of gravity; (b) Total magnetic field.

3.1.3 Case 3: joint L_1 -norm inversion with cross-gradient constraint and hard constraint matrix

The algorithm is implemented again with $\lambda = 10^6$, but now, based on available information, we suppose that the physical properties for one prism in the vertical dike, located in the upper left side, are known. These known values are communicated to the algorithm via \mathbf{m}^{apr} and by setting the corresponding entries of W_h to 100. The inversion terminates at iteration $IT = 59 < \text{MAXIT}$. The reconstructed models are presented in Figs. 12(a) and 12(b). The results are even better than those obtained by the previous reconstruction, as demonstrated by the model illustrated in Fig. 6. Here, the known model parameters are kept fixed during

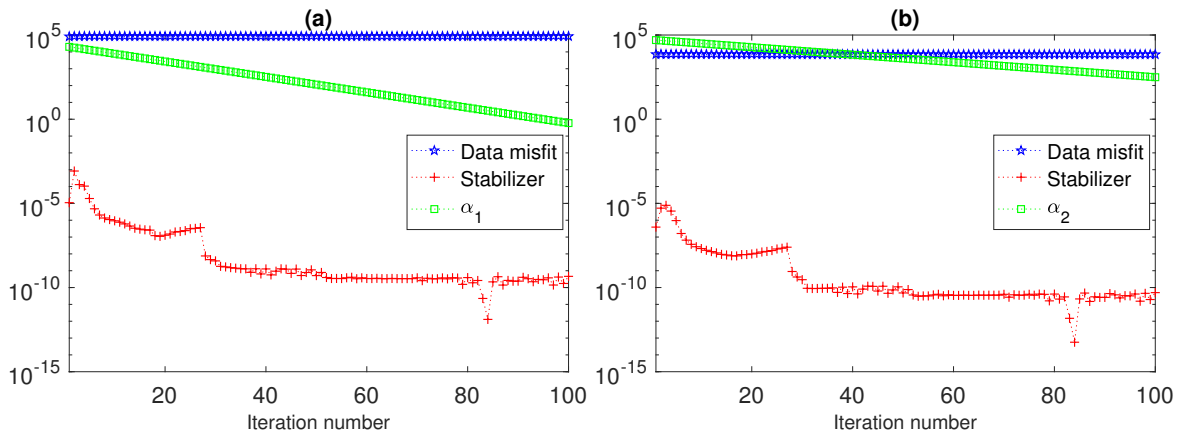


Figure 11. The progression of the data misfit, the regularization term, and the regularization parameter, with iteration ℓ , for the models shown in Fig. 9, Model 1 and Case 2. (a) Gravity; and (b) Magnetic.

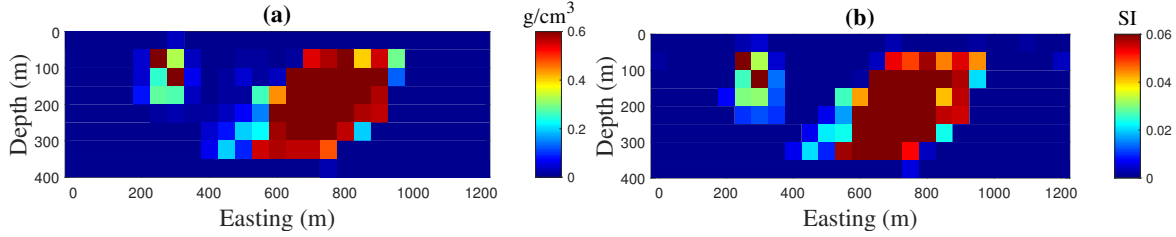


Figure 12. Reconstructed models using joint inversion with $\lambda = 10^6$, with the L_1 -norm of the model parameters as the stabilizer, and with the application of the hard constraint matrix, Model 1 and Case 3. (a) Density distribution; (b) Susceptibility distribution.

the iterations. The results demonstrate how the incorporation of available information for some model parameters can increase the reliability of the model obtained using the inverse algorithm.

3.1.4 Case 4: joint minimum structure inversion with cross-gradient constraint

For this example, we implement the joint inversion algorithm using the minimum structure stabilizer and initial regularization parameters, $\alpha_1^{(1)} = 200,000$ and $\alpha_2^{(1)} = 500,000$. These values are larger than were used for the L_1 -norm implementations discussed for Model 1 with Cases 1 to 3, in Sections 3.1.1-3.1.3. This increase in the regularization parameters is due to the significant change in the minimization function when changing the stabilizer from the L_1 -norm to the L_2 -norm. Moreover, we also use $\lambda = 10^7$ in order to increase the weighting on the cross-gradient constraint, consistently with increasing the weight on the stabilizer. All other parameters remain the same as selected for Cases 1 to 3. It is also important to note that for this simulation, even though α_1 and α_2 decrease as determined by q_1 and q_2 , the data misfit does not necessarily decrease monotonically with the iterations. Because this increase in the data misfit can occur, the algorithm is modified to hold α_1 or α_2 fixed for any iteration in which an increase in the calculated data misfit occurs. Moreover, the related model update for that iteration is rejected. Specifically, this means that the step is repeated without the decrease in the regularization parameter. This experience demonstrates that it is important to determine a reliable automatic parameter-choice strategy during the inversion, which is a complicated problem when three parameters are involved. The approach adopted here, which is quite simple but probably not optimal, leads to acceptable solutions, as compared with those presented by Fregoso & Gallardo (2009). The inversion terminates at $\text{MAXIT} = 100$. Equivalently, this means that the χ^2 tests on the noise level are not satisfied for both data sets. The results are presented in Figs. 13, 14, and 15. As expected from the use of the

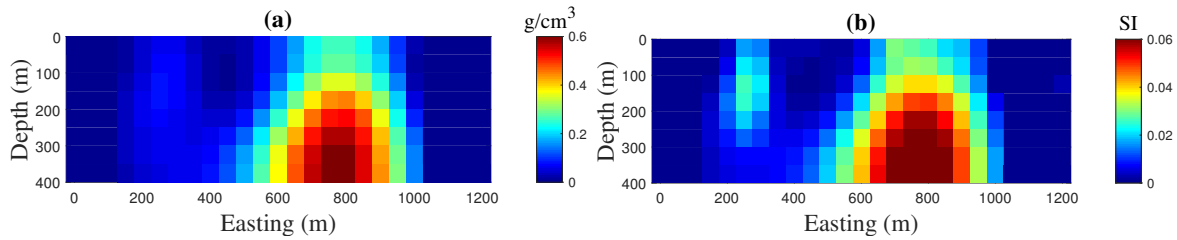


Figure 13. Reconstructed models using joint inversion with $\lambda = 10^7$ and with the L_2 -norm of the gradient of the model parameters as the stabilizer, Model 1 and Case 4. (a) Density distribution; (b) Susceptibility distribution.

minimum structure constraint, the reconstructed models are smooth. Moreover, as imposed by the use of the cross-gradient constraint, the models have a similar structure. They indicate a large dipping dike along with a small vertical structure in the subsurface. We note that the minimum structure inversion has its own advantages, which should not be disregarded, and that make the algorithm a safe strategy for the reconstruction of low-frequency subsurface structures. The progression of the data misfit, the regularization term, and the regularization parameters, with iteration ℓ , are presented in Fig. 15. These plots demonstrate that it is only at the initial iterations where there are significant changes in the parameters between successive iterative steps. Once the parameters are effectively fixed, the changes are very small, which suggests that the algorithm can be safely terminated for a smaller value of MAXIT. For direct comparison with the presented results given for Model 1 with Cases 1 to 3 we keep $\text{MAXIT} = 100$.

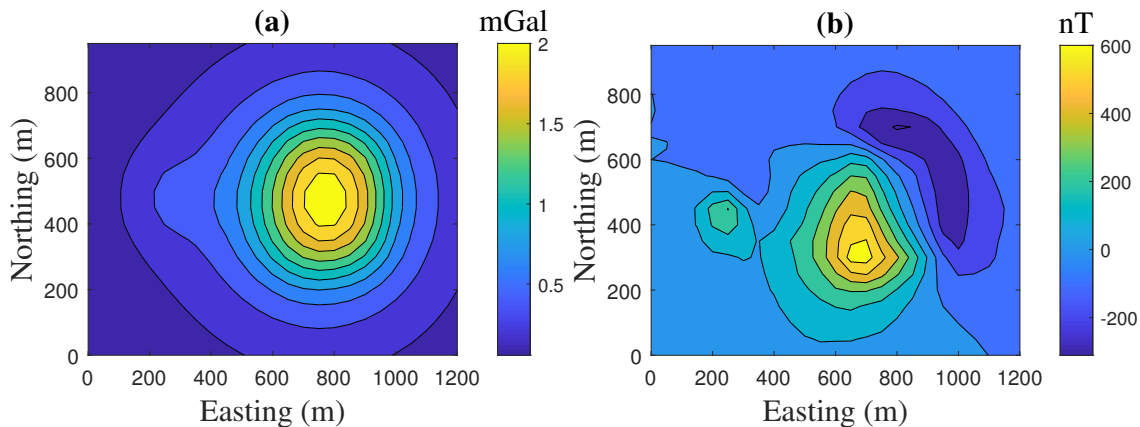


Figure 14. The data produced by the models shown in Fig. 13, Model 1 and Case 4. (a) Vertical component of gravity; (b) Total magnetic field.

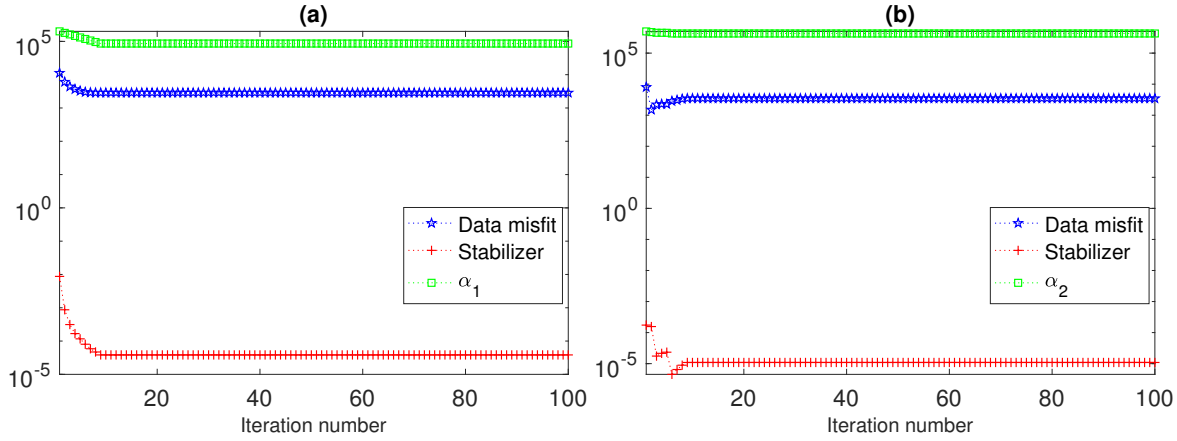


Figure 15. The progression of the data misfit, the regularization term, and the regularization parameter, with iteration ℓ , for the models shown in Fig. 13, Model 1 and Case 4. (a) Gravity; and (b) Magnetic.

3.2 Model study 2

For the second model we assume that the dipping dike has both a density and a susceptibility distribution, but that the vertical dike is not magnetic and has, therefore, only a density distribution. Figs. 16(a) and 16(b) illustrate the models. Here, the aim is to test the joint inversion algorithm, when one model has a structure in a location where the other model does not. The data produced by the models are presented in Figs. 17(a) and 17(b), respectively.

3.2.1 Case 1: joint L_1 -norm inversion with cross-gradient constraint

The joint inversion algorithm is implemented using the L_1 -norm stabilizer and with the parameters the same as were selected for the Case 2 simulation of Model 1 in Section 3.1.2. The inversion terminates at IT = 58, one iteration less than its counterpart in Section 3.1.2. The reconstructed models are shown in Figs. 18(a) and 18(b). The dipping dikes, in both density and susceptibility distributions, are reconstructed very well, and they are completely similar.

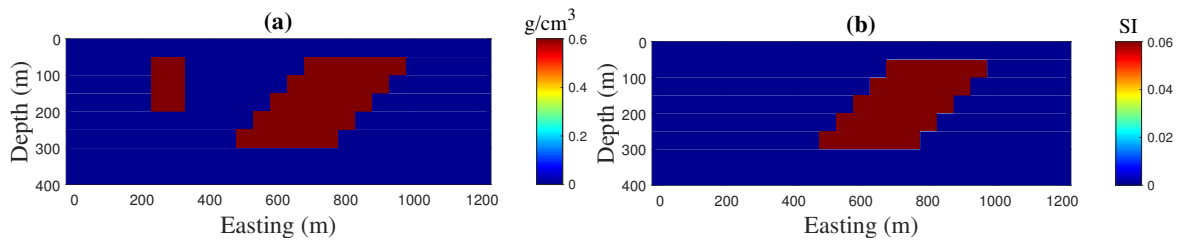


Figure 16. Cross-section of the synthetic model 2. (a) Density distribution; (b) Susceptibility distribution. Here, it is assumed that the vertical dike is not magnetic.

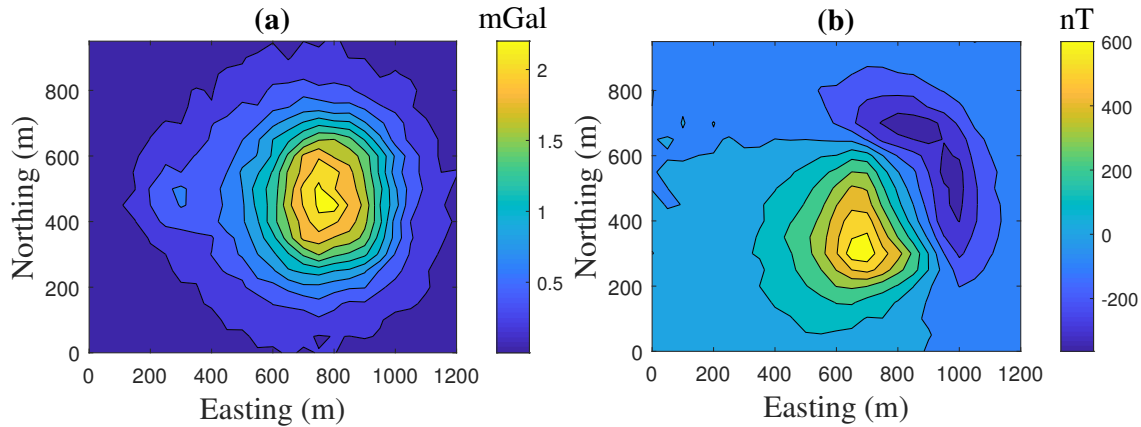


Figure 17. Noise contaminated anomaly produced by the model shown in Fig. 16. (a) Vertical component of gravity; (b) Total magnetic field. The SNR for gravity and magnetic data, respectively, are 25.1778 and 25.1773.

The density distribution of the vertical dike is almost reconstructed and no susceptibility distribution is obtained. This confirms, as noted by the theory of the cross-gradient constraint, that it is possible to reconstruct models which do not share all structures. Only the structures which are supported by the data will be similar.

3.2.2 Case 2: joint minimum structure inversion with cross-gradient constraint

For the final validation of the algorithm, we implemented the joint inversion algorithm using the minimum structure stabilizer for the data of Fig 17. All the parameters are selected as for the simulation for Model 1 with Case 4 in Section 3.1.4. The algorithm terminated at the maximum iteration, $IT = 100$. The reconstructed models are presented in Figs. 19(a) and 19(b). As for the simulation with the L_1 -norm of the model parameters in Case 1, the susceptibility model exhibits none of the structure of the vertical dike.

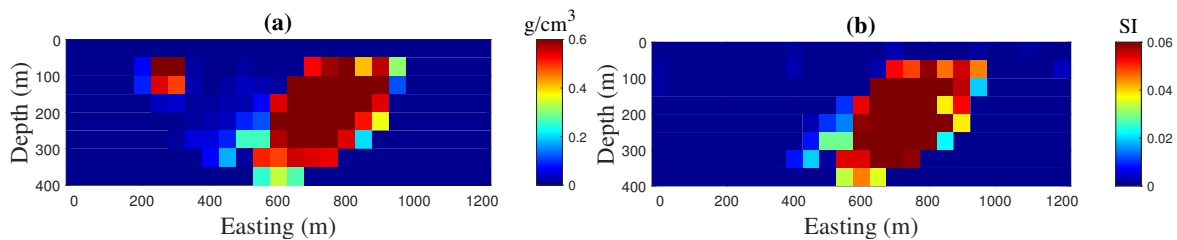


Figure 18. Reconstructed models using joint inversion with $\lambda = 10^6$ and with the L_1 -norm of the model parameters as the stabilizer, Model 2 and Case 1. (a) Density distribution; (b) Susceptibility distribution.

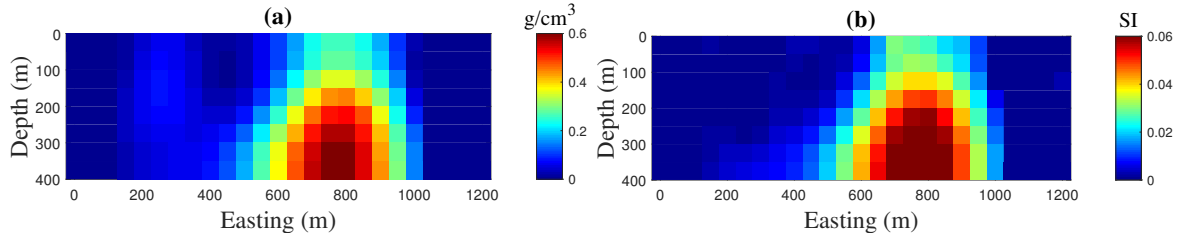


Figure 19. Reconstructed models using joint inversion with $\lambda = 10^7$ and with the L_2 -norm of the gradient of the model parameters as the stabilizer, Model 2 and Case 2. (a) Density distribution; (b) Susceptibility distribution.

4 CONCLUSIONS

A unified framework for the incorporation of the L_p -norm constraint in an algorithm for joint inversion of gravity and magnetic data, in which the cross-gradient constraint provides the link between the two models, has been developed. This unifying framework shows how it is possible to incorporate all well-known and widely used stabilizers, that are used for potential field inversion, within a joint inversion algorithm with the cross-gradient constraint. By suitable choices of the parameter p and the weighting matrix, that define the L_p -norm constraint, it is possible to reconstruct a subsurface target exhibiting smooth, sparse, or blocky characteristics. The global objective function for the joint inversion consists of a data misfit term, a general form for the stabilizer, and the cross-gradient constraint. Their contributions to the global objective function are obtained using three different regularization parameters. A simple iterative strategy is used to convert the global non-linear objective function to a linear form at each iteration, and the regularization weights can be adjusted at each iteration. Depth weighting and hard constraint matrices are also used in the presented inversion algorithm. These make it possible to weight prisms at depth, and to include the known values of some prisms in the reconstructed model. Bound constraints on the model parameters may also be imposed at each iteration.

Results presented for two synthetic three-dimensional models illustrate the performance of the developed algorithm. These results indicate that, when suitable regularization parameters can be estimated, the joint inversion algorithm yields suitable reconstructions of the subsurface structures. These reconstructions are improved in comparison with reconstructions obtained using independent gravity and magnetic inversions. The structures of the subsurface targets, for both density and susceptibility distributions, are quite similar and are close to the original models. A simple but practical strategy for the estimation of the regularization parameters is provided, by which large values are used at the initial step of the iteration, with a gradual

decrease in subsequent iterations, dependent on selected scaling parameters for each of the imposed gravity and magnetic constraint terms. The weight on the cross-gradient linkage constraint is chosen to balance to the three regularization terms. The results shows that this strategy is effective, particularly given the lack of any known robust methods for automatically estimating these parameters. The latter is a topic for our future study, as is the development of an improved implementation for the practical and efficient solution of three-dimensional large-scale problems and its application for real data.

ACKNOWLEDGMENTS

Rosemary Renaut acknowledges the support of NSF grant DMS 1913136: “Approximate Singular Value Expansions and Solutions of Ill-Posed Problems”.

REFERENCES

- Ajo-Franklin, J. B., Minsley, B. J. & Daley, T. M., 2007. Applying compactness constraints to differential travelttime tomography, *Geophysics*, **72** (4), R67-R75.
- Barbosa, V. C. F. & Silva, J. B. C., 1994. Generalized compact gravity inversion, *Geophysics*, **59** (1), 57-68, doi: 10.1190/1.1443534 .
- Bertete-Aguirre, H., Cherkaev, E. & Oristaglio, M., 2002. Non-smooth gravity problem with total variation penalization functional, *Geophysical Journal International*, **149** (2), 499-507, doi: 10.1046/j.1365-246X.2002.01664.x.
- Blakely, R. J., 1996. *Potential Theory in Gravity & Magnetic Applications*, Cambridge University Press, Cambridge, United Kingdom.
- Boulanger, O. & Chouteau, M., 2001. Constraint in 3D gravity inversion, *Geophysical Prospecting*, **49** (2), 265-280, doi:10.1046/j.1365-2478.2001.00254.x.
- Constable, S. C., Parker, R. L. & Constable, C. G., 1987. Occam’s inversion: A practical algorithm for generating smooth models from electromagnetic sounding data, *Geophysics*, **52** (3), 289-300.
- Fiandaca, G., Doetsch, J., Vignoli, G. & Auken, E., 2015. Generalized focusing of time-lapse changes with applications to direct current and time-domain induced polarization inversions, *Geophysical Journal International*, **203** (2), 1101-1112, doi: 10.1093/gji/ggv350.
- Fournier, D. & Oldenburg, D. W., 2019. Inversion using spatially variable mixed ℓ_p -norms, *Geophysical Journal International*, **218** (1), 268-282, doi: 10.1093/gji/ggz156.
- Farquharson, C. G. & Oldenburg, D. W., 1998. Nonlinear inversion using general measure of data misfit and model structure, *Geophysical Journal International*, **134** (1), 213-227, doi: 10.1046/j.1365-246x.1998.00555.x.
- Farquharson, C. G. & Oldenburg, D. W., 2004. A comparison of automatic techniques for estimating

- the regularization parameter in non-linear inverse problems, *Geophysical Journal International*, **156** (3), 411-425, doi: 10.1111/j.1365-246X.2004.02190.x.
- Fregoso, E. & Gallardo, L. A., 2009. Cross-gradients joint 3D inversion with applications to gravity and magnetic data, *Geophysics*, **74** (4), L31-L42.
- Fregoso, E., Gallardo, L. A. & Garcia-Abdeslem, J., 2015. Structural joint inversion coupled with Euler deconvolution of isolated gravity and magnetic anomalies, *Geophysics*, **80** (2), G67-G79.
- Gallardo, L. A., 2007. Multiple cross-gradient joint inversion for geospectral imaging, *Geophysical Research Letters*, **34**, L19301, doi: 10.1029/2007GL030409.
- Gallardo, L. A. & Meju, M. A., 2003. Characterization of heterogeneous near-surface materials by joint 2D inversion of DC resistivity and seismic data, *Geophys. Res. Lett.*, **30** (13), 1658, doi:10.1029/2003GL017370.
- Gallardo, L. A. & Meju, M. A., 2004. Joint two-dimensional DC resistivity and seismic travel time inversion with cross-gradients constraints, *Journal of Geophysical Research*, **109**, B03311.
- Gross, L., 2019. Weighted cross-gradient function for joint inversion with the application to regional 3-D gravity and magnetic anomalies, *Geophysical Journal International*, **217** (3), 2035-2046. doi:10.1093/gji/ggz134.
- Haáz, I. B., 1953. Relations between the potential of the attraction of the mass contained in a finite rectangular prism and its first and second derivatives, *Geofizikai Közlemenyek*, **2** (7), (in Hungarian).
- Haber, E. & Oldenburg, D. W., 1997. Joint inversion: a structural approach, *Inverse Problems*, **13**, 6377.
- Haber, E. & Gazit, M. H., 2013. Model Fusion and Joint Inversion, *Surv. Geophys.*, **34**, 675-695.
- Jorgensen, M. & Zhdanov, M. S., 2019. Imaging Yellowstone magmatic system by the joint Gramian inversion of gravity and magnetotelluric data, *Physics of the Earth and Planetary Interiors*, **292**, 12-20. doi: 10.1016/j.pepi.2019.05.003.
- Last, B. J. & Kubik, K., 1983. Compact gravity inversion, *Geophysics*, **48** (6), 713-721, doi: 10.1190/1.1441501.
- Lelièvre, P. G. & Oldenburg, D. W., 2009. A comprehensive study of including structural orientation information in geophysical inversions, *Geophysical Journal International*, **178** (2), 623-637, doi: 10.1111/j.1365-246X.2009.04188.x.
- Lelièvre, P. G. & Farquharson, C. G., 2013. Gradient and smoothness regularization operators for geophysical inversion on unstructured meshes, *Geophysical Journal International*, **195** (1), 330-341, doi: 10.1093/gji/ggt255.
- Li, Y. & Oldenburg, D. W., 1996. 3-D inversion of magnetic data, *Geophysics*, **61** (2), 394-408.
- Li, Y. & Oldenburg, D. W., 1998. 3-D inversion of gravity data, *Geophysics*, **63** (1), 109-119.
- Li, Y. & Oldenburg, D. W., 2000. Incorporating geologic dip information into geophysical inversions, *Geophysics*, **65** (1), 148-157, doi: 10.1190/1.1444705.

- Lin, W. & Zhdanov, M. S., 2018. Joint multinary inversion of gravity and magnetic data using Gramian constraints, *Geophysical Journal International*, **215** (3), 1540-1577. doi: 10.1093/gji/ggy351.
- Moorkamp, M., Heincke, B., Jegen, M., Roberts A. W. & Hobbs, R. W., 2011. A framework for 3-D joint inversion of MT, gravity and seismic refraction data, *Geophysical Journal International*, **184** (1), 477-493.
- Moorkamp, M., Roberts, A. W., Jegen, M., Heincke, B., & Hobbs, R. W., 2013. Verification of velocity-resistivity relationships derived from structural joint inversion with borehole data, *Geophysical Research Letters*, **40**, 3596-3601.
- Nabighian, M. N., Ander, M. E., Grauch, V. J. S., Hansen, R. O., Lafehr, T. R., Li, Y., Pearson, W. C., Peirce, J. W., Philips, J. D. & Ruder, M. E., 2005. Historical development of the gravity method in exploration, *Geophysics*, **70**, 63-89.
- Nielsen, L. & Jacobsen, B. H., 2000. Integrated gravity and wide-angle seismic inversion for two-dimensional crustal modelling, *Geophysical Journal International*, **140** (1), 222-232.
- Pilkington, M., 1997. 3-D magnetic imaging using conjugate gradients, *Geophysics*, **62** (4), 1132-1142.
- Portniaguine, O. & Zhdanov, M. S., 1999. Focusing geophysical inversion images, *Geophysics*, **64** (3), 874-887, doi:10.1190/1.1444596.
- Rao, D. B. & Babu, N. R., 1991. A rapid method for three-dimensional modeling of magnetic anomalies, *Geophysics*, **56** (11), 1729-1737. doi:10.1190/1.1442985.
- Sun, J. & Li, Y., 2014. Adaptive L_p inversion for simultaneous recovery of both blocky and smooth features in a geophysical model, *Geophysical Journal International*, **197** (2), 882-899, doi: 10.1093/gji/ggu067.
- Tarantola, A. & Valette, B., 1982. Generalized nonlinear inverse problems solved using the least squares criterion, *Reviews of Geophysics and Space Physics*, **20** (2), 219-232.
- Tryggvason, A & Linde, N., 2006. Local earthquake (LE) tomography with joint inversion for P- and S-wave velocities using structural constraints, *Geophysical Research Letters*, **33**, L07303, doi:10.1029/2005GL025485.
- Vatankhah, S., Ardestani, V. E. & Renaut, R. A., 2014a. Automatic estimation of the regularization parameter in 2D focusing gravity inversion: application of the method to the Safo manganese mine in northwest of Iran, *Journal Of Geophysics and Engineering*, **11** (4), 045001, doi:10.1088/1742-2132/11/4/045001.
- Vatankhah, S., Renaut, R. A. & Ardestani, V. E., 2014b. Regularization parameter estimation for underdetermined problems by the χ^2 principle with application to 2D focusing gravity inversion, *Inverse Problems*, **30**, 085002, doi: 10.1088/0266-5611/30/8/085002.
- Vatankhah, S., Renaut, R. A. & Ardestani, V. E., 2017. 3-D Projected L_1 inversion of gravity data using truncated unbiased predictive risk estimator for regularization parameter estimation, *Geophysical Journal International*, **210** (3), 1872-1887, doi:10.1093/gji/ggx274.
- Vatankhah, S., Renaut, R. A. & Ardestani, V. E., 2018a. Total variation regularization of the 3-D

- gravity inverse problem using a randomized generalized singular value decomposition, *Geophysical Journal International*, **213** (1), 695-705, doi: 10.1093/gji/ggy014.
- Vatankhah, S., Renaut, R. A. & Ardestani, V. E., 2018b. A fast algorithm for regularized focused 3D inversion of gravity data using randomized singular-value decomposition, *Geophysics*, **83** (4), G25-G34, doi: 10.1190/geo2017-0386.1.
- Vatankhah, S., Liu, S., Renaut, R. A., Hu, X. & Baniamerian J., 2019b. Improving the use of the randomized singular value decomposition for the inversion of gravity and magnetic data, *Submitted*, -, arXiv:1906.11221.
- Vatankhah, S., Renaut, R. A. & Liu, S., 2019a. A unifying framework for widely-used stabilization of potential field inverse problems, *Geophysical Prospecting*, **Under preparation**, 0-0, doi: 10.1111/1365-2478.12926.
- Wohlberg, B. & Rodríguez, P. 2007. An iteratively reweighted norm algorithm for minimization of total variation functionals, *IEEE Signal Processing Letters*, **14** (12), 948–951.
- Zhang, Y. & Wang, Y., 2019. *Three-Dimensional Gravity-Magnetic Cross-Gradient Joint Inversion Based on Structural Coupling and a Fast Gradient Method*, *Journal of Computational Mathematics*, **37** (6), 758-777. doi:10.4208/jcm.1905-m2018-0240.
- Zhdanov, M. S., 2015. *Inverse Theory and Applications in Geophysics*, Elsevier
- Zhdanov, M. S. & Tolstaya, E., 2004. Minimum support nonlinear parameterization in the solution of 3D magnetotelluric inverse problem, *Inverse Problems*, **20**, 937-952, doi: 10.1088/0266-5611/20/3/017.
- Zhdanov, M. S., Gribenko, A. & Wilson, G., 2012. Generalized joint inversion of multimodal geophysical data using Gramian constraints, *Geophysical Research Letters*, **39**, L09301, doi:10.1029/2012GL051233.

APPENDIX A: CROSS-GRADIENT FORMULATION

The components of the cross-gradient function (2) are given by

$$\mathbf{t}^x(\mathbf{m}_1(x, y, z), \mathbf{m}_2(x, y, z)) = \frac{\partial \mathbf{m}_1}{\partial y} \frac{\partial \mathbf{m}_2}{\partial z} - \frac{\partial \mathbf{m}_1}{\partial z} \frac{\partial \mathbf{m}_2}{\partial y} \in \mathcal{R}^n \quad (\text{A.1})$$

$$\mathbf{t}^y(\mathbf{m}_1(x, y, z), \mathbf{m}_2(x, y, z)) = \frac{\partial \mathbf{m}_1}{\partial z} \frac{\partial \mathbf{m}_2}{\partial x} - \frac{\partial \mathbf{m}_1}{\partial x} \frac{\partial \mathbf{m}_2}{\partial z} \in \mathcal{R}^n \quad (\text{A.2})$$

$$\mathbf{t}^z(\mathbf{m}_1(x, y, z), \mathbf{m}_2(x, y, z)) = \frac{\partial \mathbf{m}_1}{\partial x} \frac{\partial \mathbf{m}_2}{\partial y} - \frac{\partial \mathbf{m}_1}{\partial y} \frac{\partial \mathbf{m}_2}{\partial x} \in \mathcal{R}^n, \quad (\text{A.3})$$

yielding $\mathbf{t}(\mathbf{m}(x, y, z)) = \text{block_stack}(\mathbf{t}^x, \mathbf{t}^y, \mathbf{t}^z) \in \mathcal{R}^{3n}$. As illustrated in Fig. A1, the subsurface is commonly divided into right rectangular prisms. Here, we suppose all prisms have same dimensions and that $\mathbf{m}(i, j, k)$ represents the value of the current estimate for \mathbf{m} at $(x, y, z) = (i\Delta x, j\Delta y, k\Delta z)$ where $i \geq 0, j \geq 0, k \geq 0$, with the origin, $\mathbf{m}(0, 0, 0)$, at the top left corner of the domain. All other parameters indexed in the same way also correspond to the parameter

at the given grid point of the volume. We use forward difference operators for each of the derivatives in (A.1) to give .

$$\begin{aligned} \mathbf{t}^x(i, j, k) &= \left(\frac{\mathbf{m}_1(i, j+1, k) - \mathbf{m}_1(i, j, k)}{\Delta y} \right) \left(\frac{\mathbf{m}_2(i, j, k+1) - \mathbf{m}_2(i, j, k)}{\Delta z} \right) - \\ &\quad \left(\frac{\mathbf{m}_1(i, j, k+1) - \mathbf{m}_1(i, j, k)}{\Delta z} \right) \left(\frac{\mathbf{m}_2(i, j+1, k) - \mathbf{m}_2(i, j, k)}{\Delta y} \right) \\ \mathbf{t}^y(i, j, k) &= \left(\frac{\mathbf{m}_1(i, j, k+1) - \mathbf{m}_1(i, j, k)}{\Delta z} \right) \left(\frac{\mathbf{m}_2(i+1, j, k) - \mathbf{m}_2(i, j, k)}{\Delta x} \right) - \\ &\quad \left(\frac{\mathbf{m}_1(i+1, j, k) - \mathbf{m}_1(i, j, k)}{\Delta x} \right) \left(\frac{\mathbf{m}_2(i, j, k+1) - \mathbf{m}_2(i, j, k)}{\Delta z} \right) \\ \mathbf{t}^z(i, j, k) &= \left(\frac{\mathbf{m}_1(i+1, j, k) - \mathbf{m}_1(i, j, k)}{\Delta x} \right) \left(\frac{\mathbf{m}_2(i, j+1, k) - \mathbf{m}_2(i, j, k)}{\Delta y} \right) - \\ &\quad \left(\frac{\mathbf{m}_1(i, j+1, k) - \mathbf{m}_1(i, j, k)}{\Delta y} \right) \left(\frac{\mathbf{m}_2(i+1, j, k) - \mathbf{m}_2(i, j, k)}{\Delta x} \right). \end{aligned}$$

These simplify as

$$\begin{aligned} \mathbf{t}^x(i, j, k) &= \frac{1}{\Delta y \Delta z} \left(\mathbf{m}_1(i, j, k) \left(\mathbf{m}_2(i, j+1, k) - \mathbf{m}_2(i, j, k+1) \right) + \mathbf{m}_1(i, j+1, k) \left(\mathbf{m}_2(i, j, k+1) - \right. \right. \\ &\quad \left. \left. \mathbf{m}_2(i, j, k) \right) + \mathbf{m}_1(i, j, k+1) \left(\mathbf{m}_2(i, j, k) - \mathbf{m}_2(i, j+1, k) \right) \right) \quad (\text{A.4}) \end{aligned}$$

$$\begin{aligned} \mathbf{t}^y(i, j, k) &= \frac{1}{\Delta z \Delta x} \left(\mathbf{m}_1(i, j, k) \left(\mathbf{m}_2(i, j, k+1) - \mathbf{m}_2(i+1, j, k) \right) + \mathbf{m}_1(i, j, k+1) \left(\mathbf{m}_2(i+1, j, k) - \right. \right. \\ &\quad \left. \left. \mathbf{m}_2(i, j, k) \right) + \mathbf{m}_1(i+1, j, k) \left(\mathbf{m}_2(i, j, k) - \mathbf{m}_2(i, j, k+1) \right) \right) \quad (\text{A.5}) \end{aligned}$$

$$\begin{aligned} \mathbf{t}^z(i, j, k) &= \frac{1}{\Delta x \Delta y} \left(\mathbf{m}_1(i, j, k) \left(\mathbf{m}_2(i+1, j, k) - \mathbf{m}_2(i, j+1, k) \right) + \mathbf{m}_1(i+1, j, k) \left(\mathbf{m}_2(i, j+1, k) - \right. \right. \\ &\quad \left. \left. \mathbf{m}_2(i, j, k) \right) + \mathbf{m}_1(i, j+1, k) \left(\mathbf{m}_2(i, j, k) - \mathbf{m}_2(i+1, j, k) \right) \right). \quad (\text{A.6}) \end{aligned}$$

The Jacobian matrix for the cross-gradient function is given by

$$\mathbf{B} = \begin{pmatrix} \mathbf{B}_{1x} & \mathbf{B}_{2x} \\ \mathbf{B}_{1y} & \mathbf{B}_{2y} \\ \mathbf{B}_{1z} & \mathbf{B}_{2z} \end{pmatrix} = (\mathbf{B}_1, \mathbf{B}_2) \in \mathcal{R}^{3n \times 2n} \quad (\text{A.7})$$

where

$$\mathbf{B}_{ix} = \frac{\partial \mathbf{t}^x}{\partial \mathbf{m}_i}, \quad \mathbf{B}_{iy} = \frac{\partial \mathbf{t}^y}{\partial \mathbf{m}_i}, \quad \mathbf{B}_{iz} = \frac{\partial \mathbf{t}^z}{\partial \mathbf{m}_i}, \quad i = 1, 2. \quad (\text{A.8})$$

We illustrate the discrete derivative for \mathbf{t}^x with respect to \mathbf{m}_1 and \mathbf{m}_2 , first noting from (A.4) that \mathbf{t}^x is a nonlinear combination of

$$\mathbf{m}_1(i, j, k), \quad \mathbf{m}_1(i, j+1, k), \quad \mathbf{m}_1(i, j, k+1) \quad \text{and} \quad \mathbf{m}_2(i, j, k), \quad \mathbf{m}_2(i, j+1, k), \quad \mathbf{m}_2(i, j, k+1).$$

Thus, component wise, there are just three derivatives with respect to each of \mathbf{m}_1 and \mathbf{m}_2 that are nonzero; in total there are only six non zero column entries for each row of the first row block matrix $(\mathbf{B}_{1x}, \mathbf{B}_{2x})$. Specifically, we only have for row ijk the column entries pqr as given by

$$(\mathbf{B}_{1x})_{ijk,pqr} = \frac{1}{\Delta y \Delta z} \begin{cases} \mathbf{m}_2(i, j+1, k) - \mathbf{m}_2(i, j, k+1) & p=i & q=j & r=k \\ \mathbf{m}_2(i, j, k+1) - \mathbf{m}_2(i, j, k) & p=i & q=j+1 & r=k \\ \mathbf{m}_2(i, j, k) - \mathbf{m}_2(i, j+1, k) & p=i & q=j & r=k+1 \end{cases} \quad (\text{A.9})$$

$$(\mathbf{B}_{2x})_{ijk,pqr} = \frac{1}{\Delta y \Delta z} \begin{cases} \mathbf{m}_1(i, j, k+1) - \mathbf{m}_1(i, j+1, k) & p=i & q=j & r=k \\ \mathbf{m}_1(i, j, k) - \mathbf{m}_1(i, j, k+1) & p=i & q=j+1 & r=k \\ \mathbf{m}_1(i, j+1, k) - \mathbf{m}_1(i, j, k) & p=i & q=j & r=k+1 \end{cases} \quad (\text{A.10})$$

Here $(\mathbf{B}_1)_{ijk,pqr}$ indicates the row associated with grid point (x_i, y_j, z_k) , and the nonzero entries are in the relevant columns indexed by pqr . Therefore, the nonzero elements on each row are given by

$$(\mathbf{B}_1)_{ijk,\dots} = \frac{1}{\Delta y \Delta z} \left(\dots \left(\mathbf{m}_2(i, j+1, k) - \mathbf{m}_2(i, j, k+1) \right) \dots \left(\mathbf{m}_2(i, j, k+1) - \mathbf{m}_2(i, j, k) \right) \dots \left(\mathbf{m}_2(i, j, k) - \mathbf{m}_2(i, j+1, k) \right) \right)$$

$$(\mathbf{B}_2)_{ijk,\dots} = \frac{1}{\Delta y \Delta z} \left(\dots \left(\mathbf{m}_1(i, j, k+1) - \mathbf{m}_1(i, j+1, k) \right) \dots \left(\mathbf{m}_1(i, j, k) - \mathbf{m}_1(i, j, k+1) \right) \dots \left(\mathbf{m}_1(i, j+1, k) - \mathbf{m}_1(i, j, k) \right) \right).$$

These equations are consistent with (A.9) and (A.10). Furthermore, the non zero entries for two row block matrices associated with derivatives of \mathbf{t}^y and \mathbf{t}^z are obtained similarly from (A.5) and (A.6).

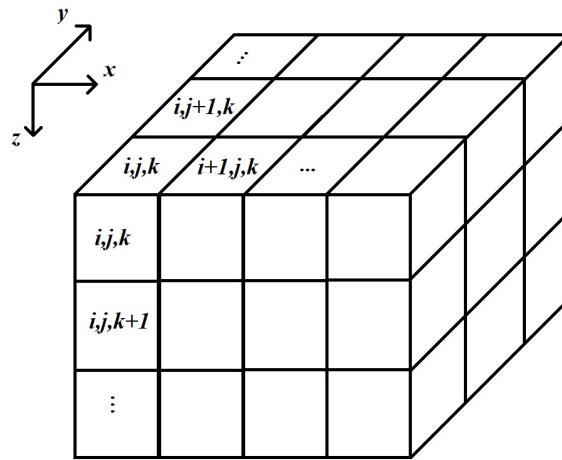


Figure A1. Discretization of the subsurface into right rectangular prisms.